

Improving physical properties of poly(vinyl alcohol)/montmorillonite nanocomposite hydrogels via the Hofmeister effect

Rongrong Guo(郭蓉蓉), Deshuai Yu(余德帅), Yifan Huang(黄一帆), Sen Wang(王森), Cong Fu(付聪), Shuihong Zhu(朱水洪), Yi Jia(易佳), Hanqi Wang(王涵淇), and Youhui Lin(林友辉)

Citation: Chin. Phys. B, 2023, 32 (**8**): 088103. DOI: 10.1088/1674-1056/acdfc2
Journal homepage: http://cpb.iphy.ac.cn; http://iopscience.iop.org/cpb

What follows is a list of articles you may be interested in

Accurate determination of anisotropic thermal conductivity for ultrathin composite film

Qiu-Hao Zhu(朱秋毫), Jing-Song Peng(彭景淞), Xiao Guo(郭潇), Ru-Xuan Zhang(张如轩), Lei Jiang(江雷), Qun-Feng Cheng(程群峰), and Wen-Jie Liang(梁文杰)

Chin. Phys. B, 2022, 31 (**10**): 108102. DOI: 10.1088/1674-1056/ac6ee5

Enhancing the thermoelectric performance through the mutual interaction between conjugated polyelectrolytes and single-walled carbon nanotubes

Shuxun Wan(万树勋), Zhongming Chen(陈忠明), Liping Hao(郝丽苹), Shichao Wang(王世超), Benzhang Li(李本章), Xiao Li(黎潇), Chengjun Pan(潘成军), and Lei Wang(王雷)

Chin. Phys. B, 2022, 31 (**2**): 028104. DOI: 10.1088/1674-1056/ac48f9

Thermoelectric characteristics of flexible reduced graphene oxide/silver selenide nanowire composites prepared by a facile vacuum filtration process

Zuo Xiao(肖佐), Yong Du(杜永), Qiufeng Meng(孟秋风), and Lei Wang(王磊)

Chin. Phys. B, 2022, 31 (**2**): 028103. DOI: 10.1088/1674-1056/ac447e

Graphene/polyaniline composite sponge of three-dimensional porous network structure as supercapacitor electrode

Jiu-Xing Jiang(姜久兴), Xu-Zhi Zhang(张旭志), Zhen-Hua Wang(王振华), Jian-Jun Xu(许健君)

Chin. Phys. B, 2016, 25 (**4**): 048102. DOI: 10.1088/1674-1056/25/4/048102

SPECIAL TOPIC — Celebrating the 100th Anniversary of Physics Discipline of Xiamen University

Improving physical properties of poly(vinyl alcohol)/montmorillonite nanocomposite hydrogels via the Hofmeister effect

Rongrong Guo(郭蓉蓉)[1], Deshuai Yu(余德帅)[1], Yifan Huang(黄一帆)[1], Sen Wang(王森)[1], Cong Fu(付聪)[1], Shuihong Zhu(朱水洪)[1], Jia Yi(易佳)[2], Hanqi Wang(王涵淇)[2], and Youhui Lin(林友辉)[1,2,†]

[1] *Department of Physics, Research Institute for Biomimetics and Soft Matter, Fujian Provincial Key Laboratory for Soft Functional Materials Research, Xiamen University, Xiamen* 361005, *China*

[2] *National Institute for Data Science in Health and Medicine, Xiamen University, Xiamen* 361102, *China*

(Received 20 April 2023; revised manuscript received 26 May 2023; accepted manuscript online 20 June 2023)

Hydrogel is a kind of three-dimensional crosslinked polymer material with high moisture content. However, due to the network defects of polymer gels, traditional hydrogels are usually brittle and fragile, which limits their practical applications. Herein, we present a Hofmeister effect-aided facile strategy to prepare high-performance poly(vinyl alcohol)/montmorillonite nanocomposite hydrogels. Layered montmorillonite nanosheets can not only serve as crosslinking agents to enhance the mechanical properties of the hydrogel but also promote the ion conduction. More importantly, based on the Hofmeister effect, the presence of $(NH_4)_2SO_4$ can endow nanocomposite hydrogels with excellent mechanical properties by affecting PVA chains' aggregation state and crystallinity. As a result, the as-prepared nanocomposite hydrogels possess unique physical properties, including robust mechanical and electrical properties. The as-prepared hydrogels can be further assembled into a high-performance flexible sensor, which can sensitively detect large-scale and small-scale human activities. The simple design concept of this work is believed to provide a new prospect for developing robust nanocomposite hydrogels and flexible devices in the future.

Keywords: nanocomposite hydrogels, Hofmeister effect, network structure, poly(vinyl alcohol), montmorillonite

PACS: 81.05.Qk, 81.07.–b

DOI: 10.1088/1674-1056/acdfc2

1. Introduction

Hydrogels are a class of widely used polymer biomaterials with a three-dimensional network structure, high water content, and tunable physicochemical properties.[1] They have been widely studied because of their potential applications in many fields, such as wound dressings,[2,3] drug delivery systems,[4] and tissue scaffolds.[5] However, due to polymer gels' network defects, most traditional hydrogels are brittle and fragile, which limits their practical applications. To overcome these drawbacks, different types of novel hydrogels with extraordinary mechanical properties have been reported, such as double network hydrogels,[6–9] topological hydrogels,[10] slide-ring hydrogels,[11] macromolecular microsphere composite hydrogels,[12] and nanocomposite hydrogels.[13,14] Recently, there has been a growing interest in nanocomposite hydrogels, which are networks of hydrated polymer chains containing dispersed nanomaterials. From previous reports, the nanoparticles in nanocomposite hydrogels are considered crosslinkers, significantly improving the mechanical performance of the networks by interacting with polymer chains via noncovalent or covalent bonds.[15] Due to the intercalation properties and nanoscale size of nanosheets, nanosheets are mainly focused on preparing nanocomposite hydrogels. To date, most known nanosheet minerals such as lithium soapstone,[16] bentonite,[17] layered double hydroxides (LDH),[18] and montmorillonite (MMT)[19,20] have been incorporated into polymer networks to manufacture nanocomposite materials for various applications. Among these nanosheets, MMT nanosheets have been widely used in industrial production and laboratory research due to being relatively simple and inexpensive. Furthermore, MMT nanosheets possess a very high specific surface area and are composed of positively charged thin sheets with a layer thickness of 1 nm and anionic balancing charges in the interlayer. Therefore, MMT nanosheets can act as multifunctional crosslinking agents, thus forming a unique network. Incorporating nanosheets into a hydrogel system synthesizes a tough nanocomposite material because highly functionalized MMT can form dense crosslinking agents, which are effective in dissipating energy and stabilizing polymer networks.

Polyvinyl alcohol (PVA) hydrogel, a physically crosslinked polymer network with tunable mechanical properties and biocompatibility, has been extensively explored for biomedical materials. Through the study, it is found that the mechanical properties of the PVA hydrogel are closely related to crystallinity. Since then, more and more studies have been done to improve the crystallinity of the PVA hydrogel, such as annealing and salting-out,[21–23] to improve the crystallinity

[†]Corresponding author. E-mail: linyouhui@xmu.edu.cn

© 2023 Chinese Physical Society and IOP Publishing Ltd

of the PVA hydrogel, which makes PVA hydrogel obtain unprecedented high strength.[24] In this work, we developed a new strategy for synthesizing PVA-MMT-$(NH_4)_2SO_4$ (PMN) nanocomposite hydrogels, which exhibit excellent mechanical properties, significant anti-swelling behavior, and outstanding electrical properties. Unlike previous works on polymer-MMT nanocomposites, we introduced the Hofmeister effect into the system by adding $(NH_4)_2SO_4$ salt solution to the PVA-MMT suspension resulting in the superior performance of PMN hydrogels compared to traditional nanocomposite hydrogels.

2. Experimental details

2.1. Materials

Polyvinyl alcohol (PVA; Sigma-Aldrich, 99%), ammonium sulphate ($(NH_4)_2SO_4$; Xilong Scientific, AR), montmorillonite (MMT; Aladdin), glutaraldehyde (Aladdin; 50%) were used. All other chemical agents were at least analytical reagent grade and used as received without further purification. Ultrapure water (18.2 MΩ; Millipore Co., USA) was used throughout the experiment.

2.2. Preparation of nanosheet composite hydrogels

PMN hydrogel First, the PVA powder was dissolved in deionized water at 100 °C and stirred for 4 hours to obtain a PVA solution (10 wt%). Different concentrations of homogeneous MMT suspensions (5/10/15/20 wt%) were also prepared by dissolving 1.05/2.20/3.55/5.00 g of MMT powder in 20 mL of deionized water at 37 °C for 6 hours. In a typical synthesis, the MMT suspension (1 mL) was added dropwise into the hot PVA solution while stirring (10 mL, 10 wt%, 70 °C). The resulting PVA-MMT solution was stirred at room temperature for 10 minutes to mix evenly. Then, the prepared $(NH_4)_2SO_4$ solution (2.0 M, 3 mL) was added into the resulting PVA-MMT solution and stirred for 5 minutes to obtain a flocculent. Last, the flocculate was transferred to a polytetrafluoroethylene mold, and the PMN hydrogel was obtained after 24 hours at room temperature. The detailed compositions of the prepared PMN hydrogels are summarized in Table 1 and are named PMN-0, PMN-5, PMN-10, PMN-15, and PMN-20, respectively.

Table 1. Composition of PMN hydrogels.

	PVA solution 10 mL	MMT solution 1 mL	$(NH_4)_2SO_4$ solution 3 ml
PMN-0	10 wt%	0 wt%	2.0 M
PMN-5	10 wt%	5 wt%	2.0 M
PMN-10	10 wt%	10 wt%	2.0 M
PMN-15	10 wt%	15 wt%	2.0 M
PMN-20	10 wt%	20 wt%	2.0 M

PMN-FT hydrogels To enhance the crystallinity of the PMN hydrogels, they were frozen at −20 °C for 24 hours and then thawed at room temperature for 24 hours, resulting in PMN-FT hydrogels.

2.3. Testing and characterization methods of nanosheet composite hydrogels

Tensile testing For the tensile tests, we used a micromechanical tester (Instron 5948) equipped with a 100 N loading cell. The samples were made into dumbbell shapes (width and thickness of 5 mm and 2 mm, respectively) and stretched using clamp attachment at a strain rate of 100 mm/min.

Compression testing For the compression tests, the hydrogels were made into cubic shapes of 10 mm×10 mm×10 mm and then set on the lower plate and compressed by the upper plate at a speed of 10 mm/min. The mechanical tester was JHY-5000 (Xiamen Jinheyuan Instrument Stock Co Ltd).

SEM and TEM characterization The hydrogel samples were imaged under a scanning electron microscope (SEM, SIGMA-HD). SEM observation was performed at an accelerating voltage of 10 kV. In addition, the MMT samples were imaged using a transmission electron microscope (TEM, JEM-1400 PLUS) with an acceleration voltage of 100 kV.

SAXS characterization A customized linear stretcher was used to hold the sample in place and stretch it as required to perform the measurements. SAXS tests were performed using Xeuss 2.0.

Rheological testing Freshly prepared PMN hydrogel was used for rheological experiments. The rheological behavior of the hydrogel was analyzed using a rheometer (Anton Paar, MCR302). The constant strain of the PMN hydrogel was 0.5%. Dynamic frequency sweeps were performed at angular velocities ranging from 0.01 Hz to 100 Hz. All rheological measurements were performed in triplicate and at 25 °C.

Swell testing To evaluate the swelling behavior of the hydrogel, fresh gel samples (10 mm×10 mm×10 mm) were soaked in 100 mL of deionized water and then removed from the deionized water. The weight of the gel samples was recorded after drying the surface with soft paper. The process was repeated until no further weight increased, and the equilibrium swelling ratio was calculated as $m/m_0 = (m_w - m)/m$, where m_w and m represent the mass of the hydrogel sample in the swollen and the initial states, respectively.

Conductivity and sensor measurements Conductivity and sensor performance were tested using a bridge tester (TH2829A) and a mechanical tester (JHY-5000). Samples were tailored to 40 mm length, 5 mm width, and 2 mm thickness. Human motion monitoring was performed with the help of volunteers who were protected by tape and gave informed consent for the tests. The tape was harmless to the volunteers.

2.4. Molecular dynamics simulation and computational details

A LAMMPS software platform with OPLSAA force field was employed for all the MDs simulation and calculation (see supporting information for more details).

3. Results and discussion

3.1. Synthesis of PMN hydrogels

As shown in Fig. 1, PMN hydrogels can be prepared through a simple one-pot process. In our experiment, MMT nanosheet was chosen as a typical nanomaterial to construct nanocomposite hydrogels since it is considered an excellent physical crosslinking agent that can improve the stability of the network structures of polymers, such as PVA (Fig. S1). The structure of MMT and the corresponding TEM image are shown in Figs. S1 and S2. In a typical synthesis, 1 mL of an MMT solution with a certain concentration was added to 10 mL of the pre-prepared PVA solution (10 wt%) and mixed under stirring in a water bath (Figs. S3 and S4). Then, 3 mL of an $(NH_4)_2SO_4$ solution was added to the PVA/MMT suspension to form the PMN flocculation state as shown in Fig. S5. As $(NH_4)_2SO_4$ was introduced into the polymer network, the Hofmeister effect caused the folding and precipitation of PVA polymer chains, thereby enhancing the hydrogel.[21] Figure S6 shows the structural evolution along with the experimental procedure. Finally, the flocculates were transferred to a polytetrafluoroethylene mold, and the PMN hydrogels with different concentrations of MMT were obtained after 24 hours at room temperature.

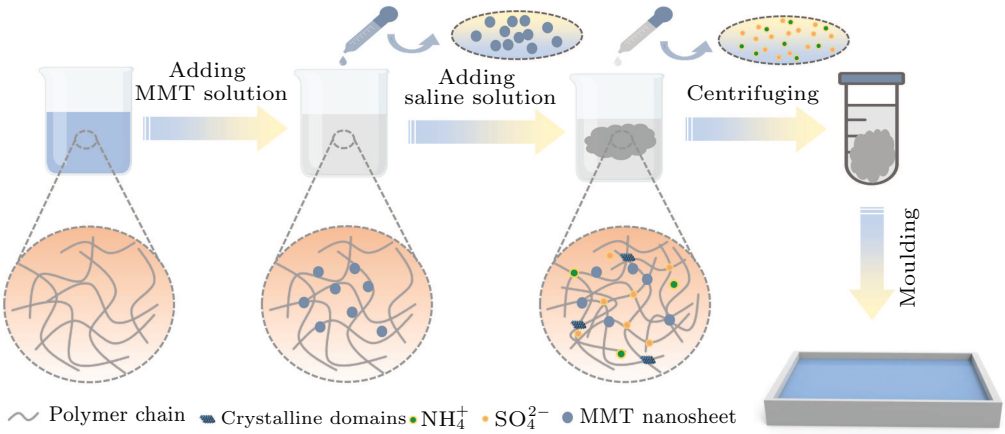


Fig. 1. Schematic diagram of the preparation process of PMN hydrogels.

3.2. Characterization of the mechanical properties of PMN

The stress–strain curve was studied to test the mechanical properties of PMN hydrogels, which show the ultimate stress and strain of PMN hydrogels (Figs. 2(b) and 2(c)). The tensile strength and elongation at the break of the hydrogel increase with the increase of MMT nanosheet content, with PMN-20 hydrogel having the highest elongation at a break of 4.89 mm/mm and tensile strength of 1.24 MPa. In addition, the PMN hydrogel without montmorillonite nanosheets has the slightest ultimate stress and strain. The stress–strain curve shows that the toughness of PMN hydrogels increases with increased MMT nanosheet content, as shown in Fig. 2(d). Specifically, when adding 1 mL of 20 wt% MMT solution, the toughness increases from 0.7 MJ/m^3 to 3.8 MJ/m^3. The addition of montmorillonite nanosheets enhances the ultimate stress, ultimate strain, and toughness of the material.

Figure 2(a) shows a schematic diagram of the internal network of the PMN hydrogel. Interestingly, the PMN hydrogel has attractive free-shapeable properties to be appropriate for customized shapes, as shown in Fig. S7.

The compression stress–strain curves of PMN hydrogels with different montmorillonite nanosheet contents are shown in Fig. 2(e). The results show that PMN-20 hydrogel with montmorillonite nanosheet layers has excellent compression performance. As shown in Fig. 2(f), the compression of Young's modulus also increases with the increase of montmorillonite nanosheet content. The compression Young's modulus refers to the slope of the stress–strain curve at 5%, 25%, and 50% strain. The results show that PMN hydrogels have high toughness and elastic modulus, and montmorillonite nanosheets as crosslinkers have a good reinforcement effect on PMN hydrogels.[25]

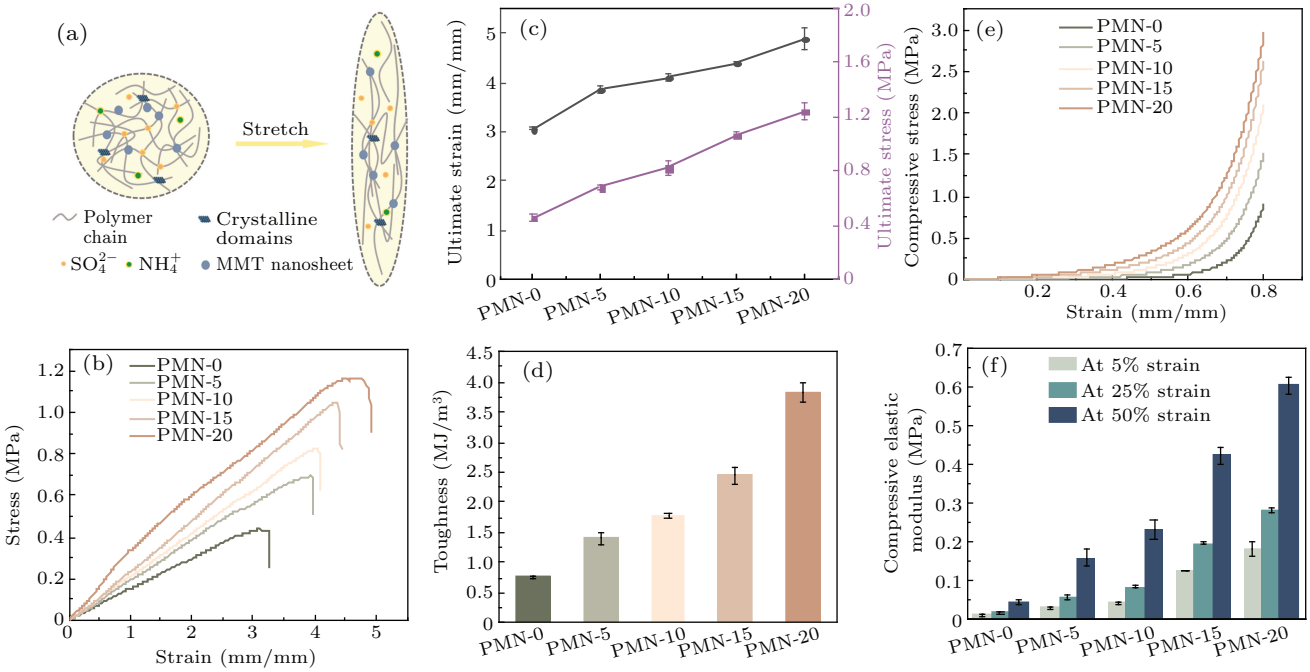


Fig. 2. (a) Schematic diagram of the network structure of PMN hydrogels during stretching. (b) The tensile stress–strain curves of PMN hydrogels containing different MMT contents. (c) Relationship between ultimate stress and strain of different PMN hydrogels. (d) The effect of montmorillonite content on the toughness of PMN hydrogels. (e) Compression stress–strain curves of different PMN hydrogels. (f) Compression elastic modulus of different PMN hydrogels with contents and strain.

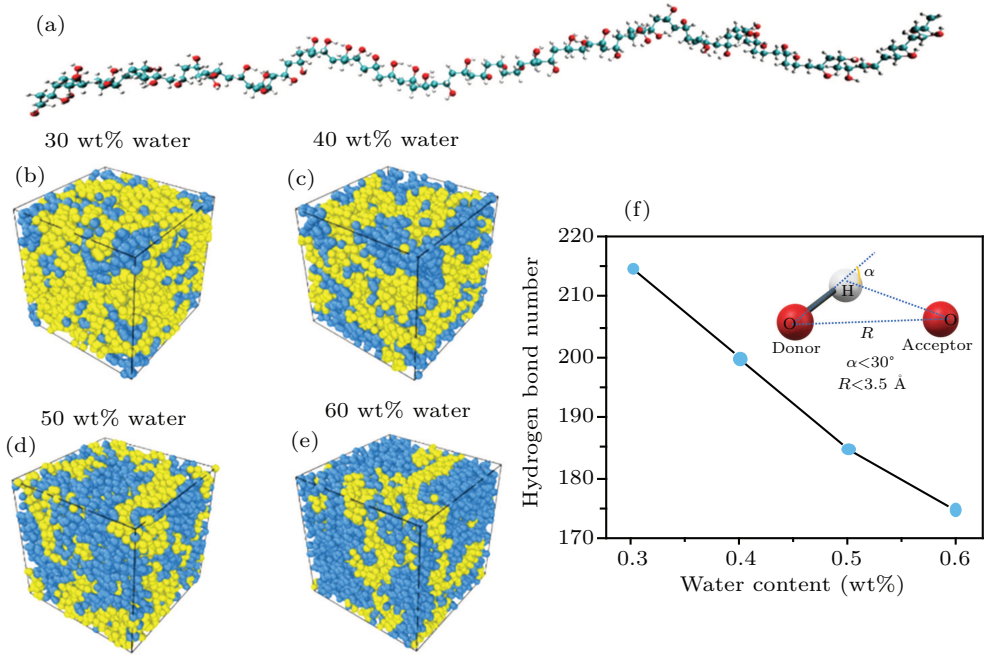


Fig. 3. (a) PVA polymer chain with a polymerization degree of 60. (b)–(e) The simulation box with 30 wt% water, 40 wt% water, 50 wt% water, 60 wt% water. The yellow part represents PVA polymers, while the blue part represents water molecules. (f) Influence of water content on the number of hydrogen bonds formed between PVA chains. The illustration shows the criteria for judging the formation of hydrogen bonds.

Due to the salting-out effect, sufficient hydrogen bonds are formed, leading to strong aggregation and partial crystallization of PVA polymer chains. The crystalline domains act as high-functional crosslinkers, enhancing and improving the structure and toughness of the material. In addition, the salting-out effect breaks the hydrogen bond between water molecules and PVA polymer chains and pulls out the water molecules from the polymer chains which is similar to reducing the water content in the hydrogel. By reducing the water, the probability of forming hydrogen bonds between polymer and water molecules is reduced, thus promoting the aggregation between the polymer chains. To provide insight into the influence of water content on the crystallinity of PVA hydrogel, all-atom molecular dynamics (MD) simulations were

carried out. In this simulation, we fitted the water molecules and the PVA polymer with a polymerization degree of 60 (Fig. 3(a)) in a box with periodic boundaries. Four simulation boxes were used as samples for simulation, which contained five PVA chains but contained 30 wt%, 40 wt%, 50 wt%, and 60 wt% of water, respectively. To more intuitively display the impact of changes in water content on the system structure, we represented all atoms on the PVA polymer chain with unified yellow beads. Similarly, all atoms in water molecules were uniformly represented by blue beads. After a relaxation of 100 ns, the system reached the equilibrium state. As shown in Figs. 3(b)–3(e), PVA chains are more likely to aggregate with each other at low water content. While, at high water content, the polymer chains are separated by water molecules and there is no significant aggregation. We calculated the number of hydrogen bonds formed between PVA chains using traditional geometric standards. As shown in Fig. 3(f), when the angle α of H–O$\cdots$H is less than 30° and the distance R between the donor and acceptor of the O atom is less than 3.5 Å, we believe that a hydrogen bond is formed between them. We calculated the number of hydrogen bonds formed between PVA polymers in each step within 100 ps after the system was stabilized and then calculated the average value. Changes in the hydrogen bond number between PVA chains as a function of the water content are shown in Fig. 3(f). With increasing the water content, the hydrogen bond between the PVA chains decreased from 215 to 175, which indicated that low water content can promote the formation of hydrogen bonds between PVA polymer chains. Thus, based on the result of the simulation, we can conclude that the PVA chains tend to aggregate and form hydrogen bonds at low water content.

The rheological properties of PMN hydrogels were studied using a rotational rheometer. As shown in Fig. 4, for all determined frequency ranges (0.1–100 rad/s) of each sample, the storage modulus G' value was significantly larger than the loss modulus G'' value, corresponding to the typical rheological behavior of the hydrogel. Moreover, by adjusting the content of MMT nanosheets in the PMN hydrogel nanocomposite, the mechanical properties of these hydrogels were tunable.[26] The storage and loss modulus of the PMN hydrogel increased with the addition of MMT nanosheets. As mentioned above, MMT nanosheets acted as crosslinkers. As the content of MMT nanosheets increased, the distance between the nanosheets decreased, which enhanced the crosslinking density of the PMN hydrogel and restricted the movement of polymer chains under shear stress.[19,27]

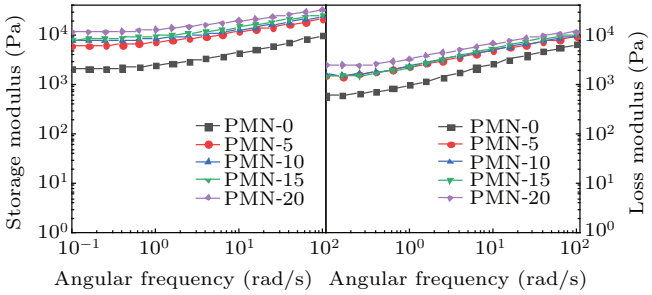


Fig. 4. The storage modulus and loss modulus of PMN hydrogels with different MMT contents.

3.3. Microstructural analysis of PMN hydrogels

To understand the internal morphology of PMN hydrogels, the surfaces of the freeze-dried PMN hydrogel samples were observed using SEM. As shown in Fig. 5, the microstructures of PMN hydrogel samples exhibited interconnected porous structures and the pore size of the hydrogel decreased with an increase in the MMT nanosheet content in the PMN hydrogel. The network structure of the PMN hydrogel became denser with an increase in the MMT content, which reduced the interstitial gaps within a unit volume and decreased the size of the pore structures.[14]

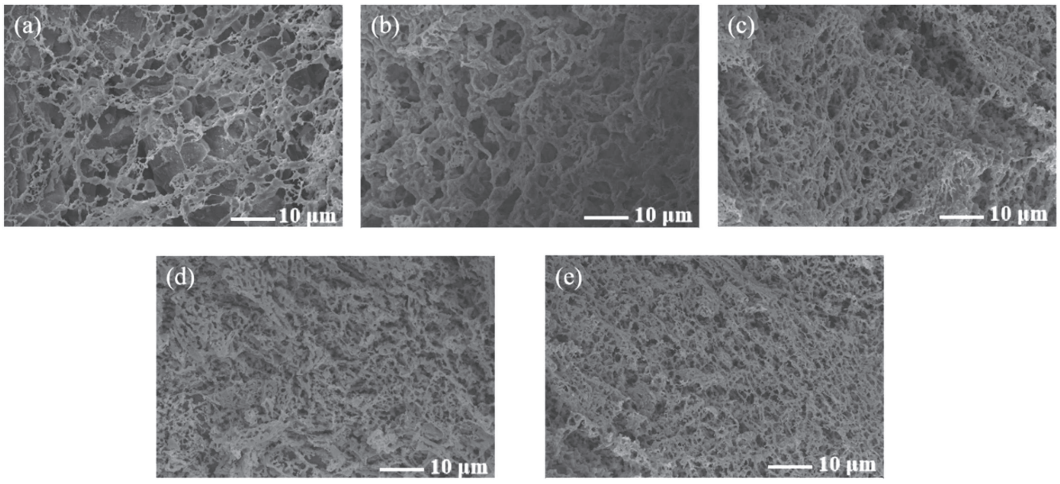


Fig. 5. (a)–(e) SEM micrographs of PMN hydrogels with different MMT contents: (a) PMN-0, (b) PMN-5, (c) PMN-10, (d) PMN-15, and (e) PMN-20.

3.4. Analysis of swelling performance of PMN hydrogels

The swelling behavior of PMN hydrogels in deionized water is presented in Fig. 6(a), which indicates a biphasic swelling pattern with a rapid swelling stage followed by a slow swelling stage. The influence of MMT nanosheets on the quality change rate of PMN hydrogels was also observed. As the MMT content increased, the anti-swelling behavior of PMN hydrogels enhanced, leading to a decrease in the quality change rate. As shown in Fig. 6(b), the equilibrium swelling ratio (ESR) was found to be dependent on the MMT content, with PMN-20 hydrogel showing a lower ESR value than PMN-0 hydrogel, indicating better resistance to swelling. The presence of MMT nanosheets acted as crosslinkers in the PMN hydrogel, playing an essential role in enhancing the crosslinking density of the hydrogel.[28] As a result, an increase in the MMT nanosheet content led to a higher density of the polymer network, limiting the flexibility and mobility of the polymer chains and thus improving the resistance to swelling.

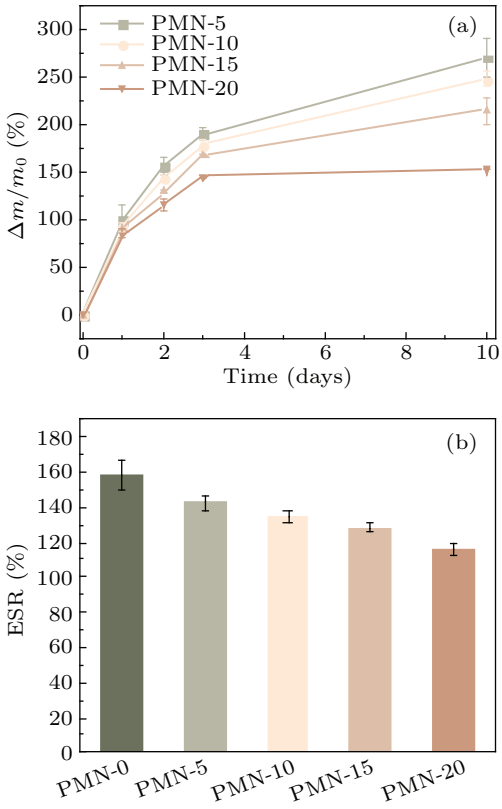


Fig. 6. (a) Swelling behavior and (b) equipment swelling ratio of PMN hydrogels with different MMT contents.

3.5. Analysis of conductive properties of PMN hydrogel

Balancing the conductivity and mechanical strength of hydrogels is still challenging. In our work, the PMN-20 hydrogel demonstrated excellent conductivity due to the formation of an ion-conductive pathway. As shown in Fig. 7, the PMN-20 hydrogel was developed as a flexible strain sensor for detecting physiological signals and human activities due to its stretchability, flexibility, high conductivity, and good biocompatibility. As shown in Figs. 7(a)–7(c), the brightness of the light-emitting diode (LED) darkens correspondingly when the hydrogel sensor is stretched and twisted. The results show that the resistance of PMN-20 hydrogel is greatly affected by tensile strain. In contrast, when PMN-20 hydrogel is twisted, the change in resistance is not significant. These PMN-20 hydrogels can convert mechanical deformation into resistance signals and may be a promising flexible material for strain sensors.[29,30]

Considering the actual situation of small strain movements in the human body, the PMN-20 strain sensor was tested at 50% and 100% strain to evaluate the reliability and repeatability of the sensing conditions. As shown in Figs. 7(d) and 7(e), the changes in relative resistance with strain were recorded, and the sensing performance was explored. To obtain $\Delta R/R_0$ with fluctuating strain, the PMN-20 strain sensor was subjected to a tensile–relaxation cycle, and the resistance recovered when the tensile strain was released. The $\Delta R/R_0$ of the strain sensor remained stable and reliable under a minor strain. At the same time, the relative resistance increased with increasing tensile strain.

Linearity and sensitivity are essential and challenging parameters for strain sensors, as they highly depend on the coordinated deformation of the hydrogel and conductive network. As shown in Fig. 7(f), the relative resistance change exhibits good linearity within a broad sensing range. The resistance change during the deformation of the PMN-20 sensor is attributed to the variation of the 3D conductive interconnect network of ion transport. The uniformly dispersed montmorillonite nanoplatelets, dissociated NH_4^+ and SO_4^{2-} in the PMN-20 hydrogel, form a well-connected conductive network.[31,32] Therefore, the developed PMN-20 strain sensor has good sensing performance, with a GF value (2.34) higher than that of traditional hydrogel sensors (GF < 0.5). Compared with the disordered structure of traditional PVA hydrogel, the layered structure of montmorillonite nanoplates can provide directional channels in the PVA network, thereby enabling more effective ion migration.

Given the excellent performance of PMN-20 hydrogel, such as electrical stability, significant sensitivity, and fast response ability, this hydrogel shows potential application prospects in wearable sensing devices. Therefore, the hydrogel strain sensor was installed on the human body to monitor joint movement. As shown in Fig. 7(g), the PMN-20 hydrogel strain sensor was tied to the finger joint, and the relative resistance change response signal increased when the finger was bent from the straight state to 90°. In addition, during the cyclic bending and straightening process, the resistance change exhibited good reversibility and fast response. This indicates the PMN-20 hydrogel sensor's ultra-fast response and excellent strain sensitivity in the slight vibration of joint deformation.

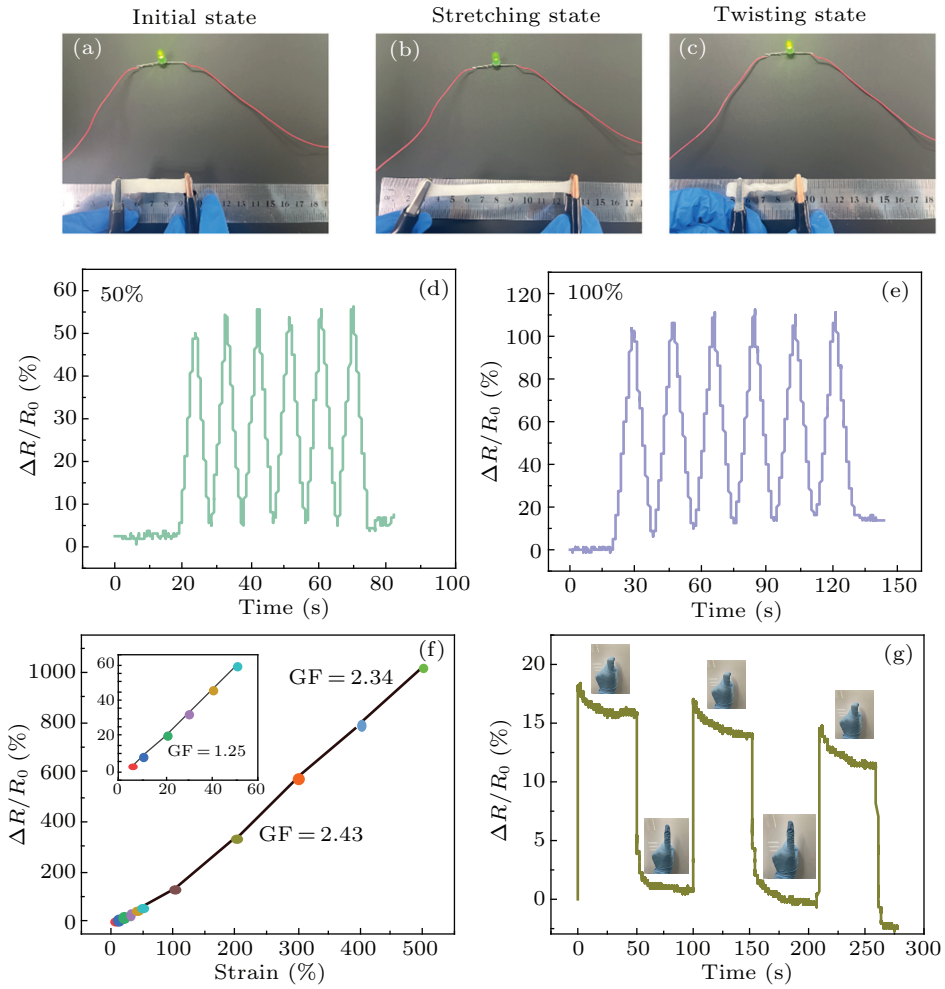


Fig. 7. (a)–(c) The excellent conductivity of PMN-20 hydrogel under different states. (d)–(e) The variation of relative resistance with (d) 50% strain and (e) 100% strain. (f) Relative resistance variation–strain curve of PMN-20 hydrogel. (g) The sensing performance of 0° and 90° finger bending.

3.6. PMN-FT hydrogels

To further improve the mechanical properties of the hydrogel, the PMN hydrogel was placed in a −20 °C environment for 24 hours and then thawed at room temperature for 24 hours to obtain the PMN-FT hydrogel. As shown in the schematic diagram in Fig. 8(a), the freeze-thaw process enhances the crystallinity of the hydrogel. After the freezing operation, the free movement ability of the molecular chain is significantly reduced, which allows the molecular chains to have longer contact time to produce more hydrogen bonds. A large number of hydrogen bonds promotes the formation of crystalline domains, resulting in more crosslinking points to support the three-dimensional network structure of the hydrogel.[33–35]

In addition, to evaluate the mechanical properties of the PMN hydrogel after freezing, the tensile stress–strain curve of the PMN-FT hydrogel was measured, as shown in Fig. 8(b). The mechanical properties of PMN-5FT, PMN-10FT, and PMN-15FT hydrogels are enhanced with increased montmorillonite content. However, the mechanical properties of PMN-20FT hydrogel decrease as too much montmorillonite interacts with the hydroxyl groups on the PVA chains, reducing the number of hydroxyl groups in the crystalline regions formed during the freezing process and causing a decrease in the mechanical properties of the PMN-20FT hydrogel. The toughness (Fig. 8(c)) and elastic modulus (Fig. 8(d)) of the PMN-FT hydrogel were calculated by analyzing the stress–strain curve. The toughness and elastic modulus of PMN hydrogels also reflected mechanical properties' enhancement after freezing. In addition, the ultimate stress and strain of the PMN-FT hydrogels as a function of MMT content are shown in Fig. S9. As shown in Fig. 8(e), the compressive elastic modulus of the PMN-FT hydrogel was measured under different compression strains. With the increase of compression strain, the compressive elastic modulus of the PMN-FT hydrogel increased. In addition, under different compression strains, the compressive elastic modulus of the PMN-FT hydrogel followed the same pattern as that under tension.

As shown in Fig. 8(f), the crystalline properties of the PMN/PMN-FT hydrogels were analyzed, and the results showed that as the network alignment increased during the stretching process of PMN-15 and PMN-15FT hydrogels, the nanofiber spacing significantly decreased, indicating a closer

crystalline structure in the PMN-15FT hydrogel. In addition, figure S10 shows the SAXS curve of PMN-15 and PMN-15FT hydrogels at room temperature and the scattering peak of PMN-15FT in the test range. The position of the SAXS peak usually corresponds to the period of the crystalline phase and the thickness of the crystalline layer for the layered crystal structure. Therefore, the PMN-15FT hydrogel formed a tighter crystal structure after the freezing operation.

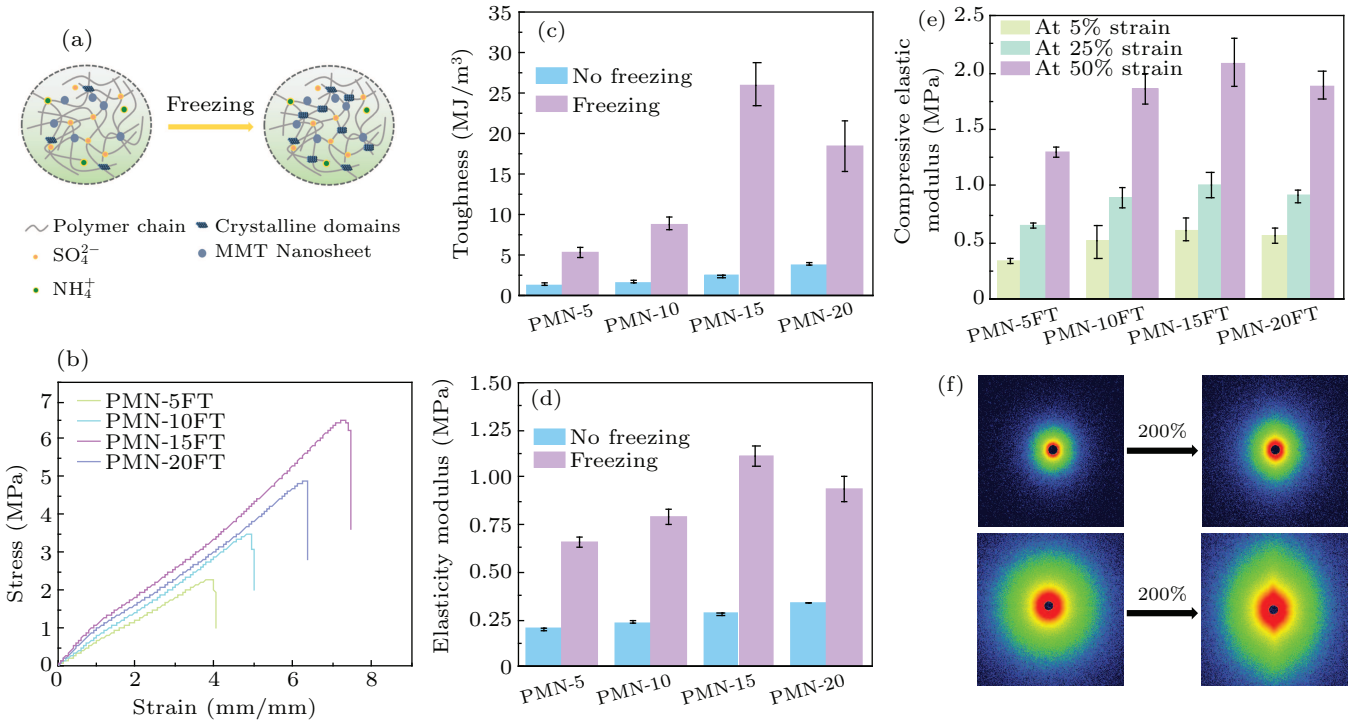


Fig. 8. (a) Illustration of the network structure of PMN-FT hydrogel. (b) The tensile stress–strain curves of PMN-FT hydrogels with different MMT contents. Comparison of (c) toughness and (d) elasticity modulus of PMN hydrogels and PMN-FT hydrogels with various MMT contents. (e) Compressive elastic modulus of PMN-FT hydrogels at different percentage strains with different MMT contents. (f) SAXS patterns of PMN-15 hydrogels (top) and PMN-15FT hydrogels (bottom) during tensile loading.

4. Conclusion

In summary, we successfully prepared Hofmeister effect-aided PMN by introducing MMT nanosheets and $(NH_4)_2SO_4$ into the PVA polymer matrix. The mechanical properties, network morphology, and swelling behavior of the PMN hydrogel can be precisely adjusted by varying the content of MMT nanosheets. With the increase of MMT nanosheet content, the mechanical performance of the PMN hydrogel is enhanced due to the increased crosslinking interaction between MMT nanosheets and polymer chains. In addition, the swelling ratio of PMN hydrogel is reduced due to the increased crosslinking degree. Furthermore, by introducing $(NH_4)_2SO_4$ into the PMN hydrogel, abundant hydrogen bonds are formed, leading to strong aggregation and crystallization of the polymer chains. In the presence of MMT nanosheets and $(NH_4)_2SO_4$, a denser PMN hydrogel network is formed, significantly improving its mechanical properties. Moreover, $(NH_4)_2SO_4$ plays an essential role in forming a dense conductive polymer network and provides the necessary amount of migrating ions. We believe this tough, anti-swelling, and conductive hydrogel will expand the potential applications of hydrogels in the field of flexible electronics.

Acknowledgements

Project supported by the National Natural Science Foundation of China (Grant No. 12274356), the Fundamental Research Funds for the Central Universities (Grant No. 20720220022), and the 111 Project (Grant No. B16029). The authors also thank Prof. Chenxu Wu, Dr. Yun Yang, and Dr. Hao Wang for valuable discussions and technical assistance.

References

[1] Meng F, Pritchard R H and Terentjev E M 2016 *Macromolecules* **49** 2843
[2] Liang Y P, He J H and Guo B L 2021 *ACS Nano* **15** 12687
[3] Zhao X D, Pei D N, Yang Y X, Xu K, Yu J, Zhang Y C, Zhang Q, He G, Zhang Y F, Li A, Cheng Y L and Chen X S 2021 *Adv. Funct. Mater.* **31** 2009442
[4] Mo F L, Jiang K, Zhao D, Wang Y Q, Song J and Tan W H 2021 *Adv. Drug Deliv. Rev.* **168** 79
[5] Maharjan B, Park J, Kaliannagounder V K, Awasthi G P, Joshi M K, Park C H and Kim C S 2021 *Carbohydr. Polym.* **251** 117023
[6] Xu X W, Jerca V V and Hoogenboom R 2021 *Mater. Horizons* **8** 1173
[7] Yang Y Y, Wang X, Yang F, Shen H and Wu D C 2016 *Adv. Mater.* **28** 7178
[8] Sun W, Xue B, Li Y, Qin M, Wu J, Lu K, Wu J, Cao Y, Jiang Q and Wang W 2016 *Adv. Funct. Mater.* **26** 9044
[9] Mu Q, Cui K, Wang Z J, Matsuda T, Cui W, Kato H, Namiki S, Yamazaki T, Frauenlob M, Nonoyama T, Tsuda M, Tanaka S, Nakajima T and Gong J P 2022 *Nat. Commun.* **13** 6213

[10] Yang J, Bai R and Suo Z 2018 *Adv. Mater.* **30** 1800671
[11] Dikshit K and Bruns C J 2021 *Soft Matter* **17** 5248
[12] Huang T, Xu H G, Jiao K X, Zhu L P, Brown H R and Wang H L 2007 *Adv. Mater.* **19** 1622
[13] Sui B W, Li Y F and Yang B 2020 *Chin. Chem. Lett.* **31** 1443
[14] Li C P, Mu C D, Lin W and Ngai T 2015 *ACS Appl. Mater. Interfaces* **7** 18732
[15] Wang Q M and Gao Z M 2016 *J. Mech. Phys. Solids* **94** 127
[16] Ling J, Li N, Yang X, Ma J J, Du J, Wang D, Tan Y, Yue F and Xu S M 2017 *J. Appl. Polym. Sci.* **134** 44963
[17] Lee W F and Chen Y C 2004 *J. Appl. Polym. Sci.* **91** 2934
[18] Radu I C, Vasile E, Damian C M, Iovu H, Stanescu P O and Zaharia C 2018 *Mater. Plast.* **55** 263
[19] Su X, Mahalingam S, Edirisinghe M and Chen B Q 2017 *ACS Appl. Mater. Interfaces* **9** 22223
[20] Gao G, Du G, Sun Y and Fu J 2015 *ACS Appl. Mater. Interfaces* **7** 5029
[21] Wu S, Hua M, Alsaid Y, Du Y, Ma Y, Zhao Y, Lo C Y, Wang C, Wu D, Yao B, Strzalka J, Zhou H, Zhu X and He X 2021 *Adv. Mater.* **33** 2007829
[22] Hua M, Wu S, Ma Y, Zhao Y, Chen Z, Frenkel I, Strzalka J, Zhou H, Zhu X and He X 2021 *Nature* **590** 594
[23] He Q, Huang Y and Wang S 2018 *Adv. Funct. Mater.* **28** 1705069
[24] Liang X, Chen G, Lin S, Zhang J, Wang L, Zhang P, Wang Z, Wang Z, Lan Y and Ge Q 2021 *Adv. Mater.* **33** 2102011
[25] Karimi A and Wan Daud W M A 2017 *Polym. Compos.* **38** 1086
[26] Okay O and Oppermann W 2007 *Macromolecules* **40** 3378
[27] Li T, Xiang S, Ma P, Bai H, Dong W and Chen M 2015 *J. Polym. Sci. Pt. B-Polym. Phys.* **53** 1020
[28] Qi X, Zeng Q, Tong X, Su T, Xie L, Yuan K, Xu J and Shen J 2021 *J. Hazard. Mater.* **402** 123359
[29] Li Y, Xu X, Zhao L, Yu D, Chen Y, Du L and Wu X 2022 *ACS Appl. Electron. Mater.* **4** 2396
[30] Cui C, Fu Q, Meng L, Hao S, Dai R and Yang J 2021 *ACS Appl. Bio Mater.* **4** 85
[31] Chen G, Huang J, Gu J, Peng S, Xiang X, Chen K, Yang X, Guan L, Jiang X and Hou L 2020 *J. Mater. Chem. A* **8** 6776
[32] Wei J and Wang Q 2019 *Small Methods* **3** 1900558
[33] Chen Y, Li J, Lu J, Ding M and Chen Y 2022 *Polym. Test* **108** 107516
[34] Dong X, Guo X, Liu Q, Zhao Y, Qi H and Zhai W 2022 *Adv. Funct. Mater.* **32** 2203610
[35] Shen Z, Zhang Z, Zhang N, Li J, Zhou P, Hu F, Rong Y, Lu B and Gu G 2022 *Adv. Mater.* **34** 2203650